Nonlinear Waves in the Terrestrial Quasiparallel Foreshock

B. Hnat,* D. Y. Kolotkov, D. O'Connell, V. M. Nakariakov, and G. Rowlands
CFSA, Physics Department, University of Warwick, Coventry CV4 7AL, United Kingdom
(Received 4 May 2016; revised manuscript received 30 June 2016; published 2 December 2016)

We provide strongly conclusive evidence that the cubic nonlinearity plays an important part in the evolution of the large amplitude magnetic structures in the terrestrial foreshock. Large amplitude nonlinear wave trains at frequencies above the proton cyclotron frequency are identified after nonharmonic slow variations are filtered out by applying the empirical mode decomposition. Numerical solutions of the derivative nonlinear Schrödinger equation, predicted analytically by the use of a pseudopotential approach, are found to be consistent with the observed wave forms. The approximate phase speed of these nonlinear waves, indicated by the parameters of numerical solutions, is of the order of the local Alfvén speed. We suggest that the feedback of the large amplitude fluctuations on background plasma is reflected in the evolution of the pseudopotential.

DOI: 10.1103/PhysRevLett.117.235102

Introduction.—Upstream regions of quasiparallel collisionless astrophysical shocks are among the most complex plasma systems. When the magnetic field direction is quasiparallel to the shock normal, a fraction of incoming ions are reflected upstream generating an extended and turbulent foreshock. The interactions of the superthermal ions with the background plasma lead to multiscale collective dynamics which mediates energy dissipation and isotropy [1]. In the last decade, the nonlinear evolution of magnetic field fluctuations emerged as a critical ingredient of Earth's quasiparallel shock, which is cyclically reformed by generating short large amplitude magnetic field structures (SLAMS) [2] in the foreshock. These SLAMS advect downstream, decelerate, and combine to form a temporary shock front.

The advent of the multispacecraft Cluster mission combined with the more accurate numerical simulations have dramatically improved our understanding of terrestrial foreshock and, in particular, the role and the typical features of SLAMS [3]. SLAMS originate from the ultra low frequency (ULF) modes destabilized by the beams of ions reflected from the shock, propagating along the magnetic field and towards the Sun with phase speeds that are much smaller than the solar wind speed. The ULF waves are then advected towards the bow shock, experiencing refraction, due to the gradient in the diffused ion population, and achieving a large propagation angle. The relative drifts between incoming and reflected species, free energy in the density gradients of the diffused ions, and the advective nonlinearity conspire to generate isolated structures with large magnetic compression ($\delta B/B_0 > 2$). Numerical studies [4] and observations [5] put the growth rate of SLAMS at a few seconds and the observations suggest that their spatial size is larger than 1000 km [6].

There is growing evidence to suggest that SLAMS have a fine internal structure, which originates from the third-order nonlinearity within the SLAMS wave packet [7,8]. Such cubic nonlinearity introduces the dependence of phase upon the amplitude in the observed wave packets. The presence of nonlinear waves in quasiparallel foreshocks may lead to wave collapse and self-focusing [9,10], which generate strong electrostatic fields on kinetic scales. This field accelerates particles, modifying their velocity distribution function [11,12]. In warm plasmas, parametric instabilities can develop through, for example, four-wave interactions, and these may generate low frequency harmonics and proceed towards fully developed turbulence [13]. Understanding the nonlinear evolution of large amplitude Alfvén and fast magnetosonic waves, their transition to quasiparallel turbulence, as well as their coexistence with the oblique strong turbulence, is fundamental not only to the terrestrial bow shock, but also to the evolution of the interplanetary shocks [14], supernova remnants [15], the acceleration of galactic cosmic rays [16], and solar wind turbulence [17].

While the instabilities generating foreshock fluctuations may be of kinetic origin, the subsequent nonlinear evolution of a subset of these perturbations can be described by a few classes of nonlinear fluidlike evolutionary equations. These equations account for the intrinsic phenomena that affect the wave evolution, such as dispersion, nonlinearity, and dissipation, and hence are independent of the specific details of various generation mechanisms. Finite amplitude dispersive slow and fast magnetosonic waves propagating at large oblique angles with respect to the magnetic field, obey the Korteweg–de Vries (KdV) equation [18]. For parallel and nearly parallel propagating Alfvén and fast magnetosonic fluctuations, the derivative nonlinear Schrödinger (DNLS) equation proved to be a good description [19–22]. Beyond magnetohydrodynamics (MHD) approximations, high-frequency nonlinear fluctuating structures on the whistler dispersion branch,

exhibiting solitonlike features, have been identified in numerical and analytical studies, e.g., Refs. [23,24].

We examine the foreshock region of the quasiparallel terrestrial bow shock and, for the first time, quantify propagation characteristics and spatial structure of nonlinear waves by direct comparison of experimental observations and numerical solutions. We find nonlinear wave trains with periods of several seconds and with speeds consistent with the background plasma Alfvén speeds. Numerical analysis confirms that the nonlinear wave forms found in observations agree with the numerical solutions of the DNLS.

Experimental data and methodology.—The data set corresponds to a foreshock crossing by the Cluster tetrahedron on February 20, 2002 at 16:56–17:52 UT. We examine three subintervals, hereafter referred to as I1, I2, and I3, each a few tens of seconds long. We use magnetic field measurement of ~22.4 samples per second from the Cluster FGM instrument [25] and 4 second averaged measurements of plasma parameters from the CIS-HIA instrument [26]. The transverse magnetic field fluctuations are obtained using minimum variance coordinates, which is equivalent to solving an eigenvalue problem for the measured magnetic field variance matrix [27].

Figure 1 shows the summary plot of key macroscopic plasma parameters as well as the omnidirectional H^+ flux (color) at different energies. The H^+ flux (bottom panel) shows a broad high energy ion component between 10^3–10^4 eV. The Cluster CIS instrument was operating in the magnetospheric mode, in which the instrument samples all angular directions. This leads to the solar wind population dominating the spectrum at the energy ~10^3 eV.

The magnitude of the transverse magnetic field components is processed using the Hilbert-Huang transform

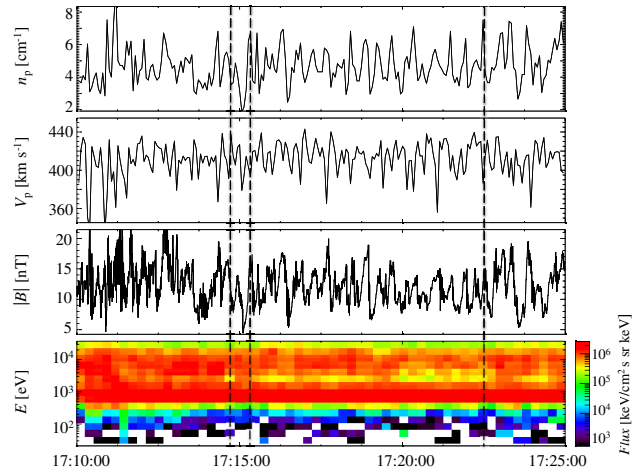

FIG. 1. Summary of Cluster observations for the interval of interest. Panels from top to bottom show: solar wind ion plasma number density, solar wind ion bulk speed, magnetic field magnitude and the omnidirectional proton flux spectrum. Vertical dashed lines mark the start of intervals I1, I2, and I3.

(HHT) spectral technique [28], which is designed for analyzing nonstationary and nonharmonic fluctuations. Unlike traditional spectral methods based on the Fourier decomposition and wavelets, which are restricted by an *a priori* assignment of harmonic basis functions, the HHT technique uses the empirical mode decomposition (EMD), which expands the given signal onto a set of intrinsic modes derived directly from the data. The stability of intrinsic modes is evaluated using the noise-assisted ensemble empirical mode decomposition (EEMD) [29]. Each EEMD trial consists of the intrinsic modes of a dummy signal obtained by adding artificial small-amplitude white noise to the original data. Ensemble averaging of these independent realizations leads to frequency stabilization, while the effect of the white noise is statistically cancelled. We note that we do not examine each empirical mode separately, but rather use this technique as a filter allowing us to find a nonharmonic trend in the signal, which can then be subtracted. This is an essential step, which allows us to examine fluctuations on scales smaller than these of SLAMS.

Results.—Figures 2–4 show nonlinear large amplitude quasiparallel transverse waves for intervals I1, I2, and I3, respectively. Panel (a) of each figure shows the squared magnitude of the original transverse fluctuations, $B_t^2(t)$, in black and a nonharmonic trend, $T(t)$, determined with the EEMD technique, in red. We subtract this trend from the original signal and normalize the residue by the mean value of the first and the last point of the trend. This new signal,

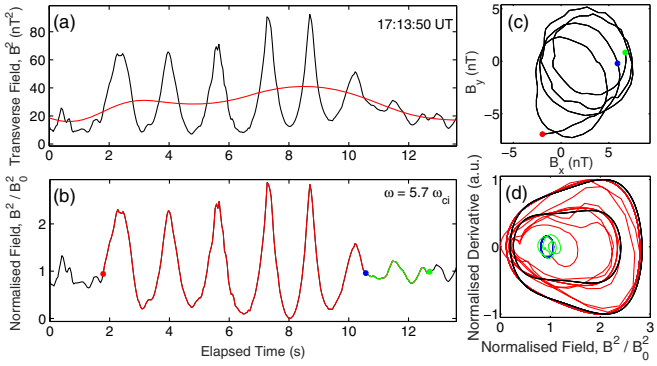

FIG. 2. Nonlinear wave forms in the magnitude of the transverse magnetic field fluctuations for interval I1. Panel (a): Original squared magnitude of transverse fluctuations (black) and the trend (red). Panel (b): Normalized and detrended signal with color dots marking the start of nonlinear waves (red), the end of the nonlinear waves or start of small amplitude waves (blue), and the end of small amplitude waves (green). The mean spacecraft frame frequency of the signal (red) is given in the top right corner. Panel (c): Hodograms of the transverse components used in (a). Panel (d): The phase space of the signal shown in (b) with the same color scheme and the equivalent trajectories obtained from the numerical solutions of Eq. (2) for parameters: $C_b = 18.9$, $V = 5.1$, $C = 3.7$ (nonlinear solution, black) and $C_b = 3.91$, $V = 8$, $C = 7.2$ (small amplitude solution, blue).

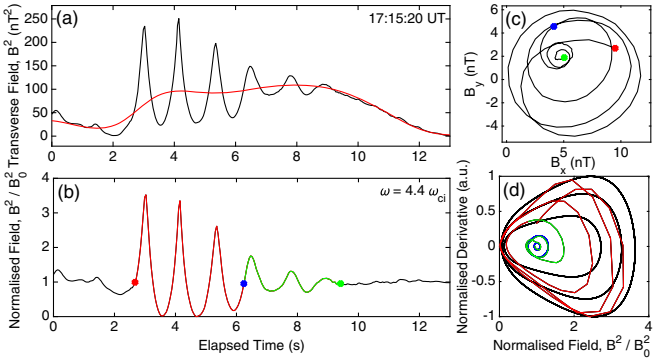

FIG. 3. Same as Fig. 2 for interval I2. Parameters of numerical solutions: $C_b = 25.08$, $V = 4.3$, $C = 3.7$ (nonlinear solution, black) and $C_b = 5.31$, $V = 8$, $C = 7.2$ (small amplitude solution, blue).

$S(t) = 2[B_t^2(t) - T(t)]/[T(1) + T(N)]$, where N is the number of points in the signal, is plotted in panel (b) of each figure. We determine the mean frequency in the spacecraft frame, in units of the mean proton gyrofrequency ω_{ci}, for the nonlinear (red) signal and these are given in the top right-hand corner of each panel (b). We mark the start of the nonlinear waves (red), end of nonlinear waves and transition to small amplitude fluctuations (blue), and the end of small amplitude fluctuations (green). Panels (c) show hodograms of the minimum variance transverse components of the magnetic field, which are left-hand polarized for all intervals, in the spacecraft frame of reference. Previous studies found modes propagating predominantly away from the bow shock for this foreshock crossing [3,30], which implies a reversed sense of polarization with respect to the plasma frame of reference, indicating that the observed fluctuations are fast magnetosonic waves. This is consistent with the polarization parameter used in the numerical solution presented below. Panels (d) show the phase plane of the signal, using the color scheme of panel (b), and the equivalent trajectories

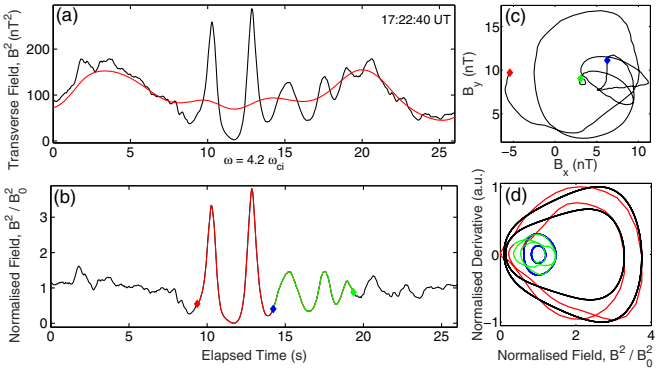

FIG. 4. Same as Fig. 2 for interval I3. Parameters of numerical solutions: $C_b = 20.25$, $V = 5.1$, $C = 4.8$ (nonlinear solution, black) and $C_b = 7.33$, $V = 9$, $C = 8.4$ (small amplitude solution, blue).

obtained from numerical solutions, which we will discuss in the next section, in black and blue. First, we comment on the nonharmonic trends identified using the EEMD technique in each example. These have a variability of tens of seconds, which coincides with the period of the ULF waves [31]. We emphasize the importance of the EMD technique and its ability to extract this nonharmonic trend, which is critical in obtaining the statistically stationary nonlinear wave trains presented here.

The main results of this work are contained in panels (b) and (d) of each figure. In each example, we are able to identify large amplitude nonlinear wave forms (red lines) which are approximately circularly polarized, span several cycles, and have a characteristic shape, with round minima and narrowly peaked maxima. Their amplitude is a factor 2–3 times larger than the background magnetic field and their periods (in the spacecraft frame of reference) are a factor 0.18–0.24 shorter than that of the ion cyclotron motion. We note, however, that in terms of the amplitude of transverse magnetic field components, B_t, the ratio $\delta B_t/\langle B_t \rangle$ is in the range of 15%–30%, for all intervals considered here. For all three examples, the nonlinear wave train is followed by small amplitude nearly harmonic oscillations (green lines). Since the solar wind velocity is of order of 400 km/s, that is much higher than the local Alfvén speed, the Taylor's hypothesis implies that we do not observe the temporal evolution of these waves, rather their spatial structure. Using the average solar wind velocity of 420 km/s, the observed periods indicate spatial gradients of approximately 200 km, in agreement with previous Cluster observations [6].

Discussion and conclusions.—We now consider the DNLS equation as a possible model for the observed nonlinear waves. Consider a magnetized plasma with elliptically polarized Alfvén or magnetoacoustic waves propagating in the quasiparallel z direction perturbing the transverse components of the magnetic field, $\mathbf{b} = b_x + ib_y$. We define the sound speed, $c_s^2 = \gamma k_B T/m_i$ and the Alfvén speed $c_A^2 = B_0^2/(\mu_0 n_i m_i)$, where γ is the adiabatic index, T is the temperature, n_i is the proton number density, and m_i is the proton mass. The evolution of these left- and right-hand polarized modes, is described by the DNLS equation [22]

$$\frac{\partial \mathbf{b}}{\partial t} + \alpha \frac{\partial}{\partial z}(\mathbf{b}|\mathbf{b}|^2) - i\mu \frac{\partial^2 \mathbf{b}}{\partial z^2} = 0. \quad (1)$$

In Eq. (1) the temporal and spatial variables have been normalized by the ion gyrofrequency, $\omega_i \equiv eB_0/m_i$, and the ion inertial length c_A/ω_i, respectively. The constant $\alpha \equiv c_A^2/[4(c_A^2 - c_s^2)]$, and $\mu = \pm 1/2$ corresponds to left (−) and right-hand (+) polarized mode. The transverse components of the magnetic field are then expressed as $\mathbf{b} = b\exp(i\Theta)$, with the phase $\Theta(t,\phi) = -\Omega t + P(\phi)$, where Ω is a constant, P is an *a priori* unknown function,

and $\phi \equiv (1/\mu)(z - Vt)$ represents the change of the frame of reference to that travelling at the phase speed of the perturbation, V (normalized by c_A). One finds the first integral of the phase equation to be $2sdP/d\phi = C + Vs - 3s^2$, where $s = \alpha b^2/2$ and C is a constant.

The equation for the magnitude of the magnetic field transverse components, expressed in the new variable s, takes the following form:

$$F(s)\frac{d^2s}{d\phi^2} + \frac{dF(s)}{ds}\left(\frac{ds}{d\phi}\right)^2 = -\sqrt{\frac{2s}{\alpha}}G(s), \qquad (2)$$

where $F(s) = 1/\sqrt{2\alpha s}$ and $G(s) = \Omega\mu + VdP/d\phi - 2sdP/d\phi - (dP/d\phi)^2$. The first integral of Eq. (2) can then be found using Bernoulli's method, which gives

$$\frac{1}{2}\left(\frac{1}{\sqrt{2\alpha s}}\frac{ds}{d\phi}\right)^2 + U_b = C_b, \qquad (3)$$

where

$$U_b = \frac{1}{4\alpha}\left(s^3 - 2Vs^2 + (4\Omega\mu + V^2 + 2C)s + \frac{C^2}{s}\right), \qquad (4)$$

and C_b is a new constant of integration. Treating s and ϕ as a generalized coordinate and time of a pseudoparticle, the first and second terms on the left-hand side of Eq. (3) represent generalized kinetic and potential energies written in the canonical form, and the constant of integration C_b can be interpreted as the total energy of a particle, which depends only on the initial conditions [32]. The form of U_b clearly shows that $U_b \to \infty$ when $s \to 0$ and when $s \to \infty$, so the solutions of Eq. (1) are oscillatory for arbitrarily large amplitudes. In order to compare the oscillatory solutions of Eq. (1) with the nonlinear wave forms found in the terrestrial foreshock, we solve Eq. (2) numerically for different initial conditions and using experimentally measured plasma parameters.

Panels (d) of Figs. 2–4 show a direct comparison of the numerical and experimental phase space trajectories. Numerical solutions were obtained for different initial energies, C_b, set to values that match the observations shown in Figs. 2–4, and with $\mu = 1/2$, $\Omega = 1$ and $\alpha = 1$. We note that the proton number density measurements from Cluster C3 spacecraft give a plasma $\beta \approx 2.5$ for these intervals, resulting in a negative value of α. However, these measurements are likely contaminated by a dense energetic proton beam reflected from the bow shock. The NASA OMNI data give a plasma β in the range 0.75–0.9, which is consistent with the number density of ions shown in the top panel of Fig. 1 and the value of α used in numerical solutions. Clearly, there is a good agreement between experimental and numerical results, indicating that the observed fluctuations are consistent with nonlinear waves governed by the DNLS equation, rather than superposition of harmonic signals.

The speed, V, used in the numerical solutions is modified by the solar wind speed. Recalling that V is normalized to the Alfvén speed, and considering parallel propagating waves, the true phase speed of the wave is $V_{\rm ph} = Vc_A + U_{\rm sw}\cos(\Theta_{vB})$, where Θ_{vB} is the angle between the solar wind velocity and the magnetic field vectors. Using averaged values (in km/s) of $c_A = 86$, $U_{\rm sw} = 410$, $\Theta_{vB} = 141°$ for I1, $c_A = 110$, $U_{\rm sw} = 412$, $\Theta_{vB} = 140°$ for I2, and $c_A = 110$, $U_{\rm sw} = 420$, $\Theta_{vB} = 156°$ for I3, we obtain $V_{\rm ph}^{I1} = 120 \pm 36$ km/s, $V_{\rm ph}^{I2} = 157 \pm 47$ km/s and $V_{\rm ph}^{I3} = 159 \pm 48$ km/s, and the error reflects standard deviation in the solar wind velocity, density, and in the magnetic field magnitude. The phase speeds are larger than the local Alfvén speed and the waves of higher amplitude [panel (b) of Figs. 2–4] propagate faster. In each case the propagation direction is sunward. This confirms that, within the reasonable range of physical parameters, the observed fluctuations are consistent with the DNLS model.

Figure 5 shows normalized functional forms of the pseudopotential Eq. (4), which correspond to solutions plotted in the phase space panels of Figs. 2–4. In each case the value of U_b is calculated from Eq. (4) using parameter values obtained from the observational data. Dashed lines in each panel correspond to the initial condition for the outermost black trajectory (red dashed) and the outermost blue trajectories (green dashed) shown in panels (d) of Figs. 2–4. The nonlinear trajectories, plotted as solid lines in panels (d) of Figs. 2–4 correspond to the pseudopotentials with a single local minimum, which likely are transient states between the single and the double well potentials. We note that the exact form of the pseudopotential for its low values is not critical to our results since the energy of the observed nonlinear fluctuations is still much higher than any local extrema or plateau visible in the red curve of Fig. 5(c). In the classification given in Ref. [22], these fluctuations were called algebraic soliton solutions. In contrast, the linear trajectories of Figs. 2–4 represent solutions near the local equilibrium of a double-well

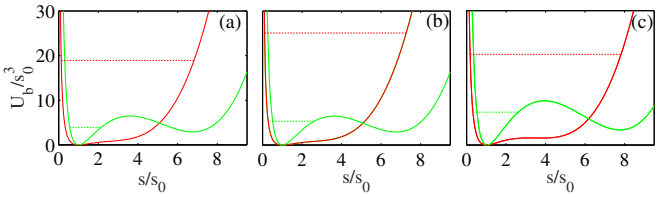

FIG. 5. The form of the potential function U_b in canonical representation for I1 (a), I2 (b), and I3(c). In all cases $\mu = 1/2$, $\Omega = 1$, and $\alpha = 1$ and other parameters are specified in the captions of Figs. 2–4. Red and green curves correspond to the nonlinear trajectories and the small amplitude fluctuations, respectively, as shown in panel (c) of Figs 2–4.

potential. A double-well potential solution corresponds to a limit of the large phase speeds V; however, the available energy in the system can only sustain small amplitude oscillations, near one of the equilibrium points. The pseudopotential reflects the properties of the medium in which the wave propagates. The change of its functional form may be interpreted as the feedback of nonlinear waves on the background plasma, but low temporal resolution of plasma data from Cluster (4s) prohibits more quantitative analysis of this phenomenon.

In summary, we have presented the first explicit detection of nonlinear waves with frequencies higher than that of the ion cyclotron and have shown that these waves are consistent with analytical predictions and numerical solutions of the DNLS equation. Our findings suggest that cubic nonlinearity, equivalent to four-wave interactions in the weak turbulence approach, is an essential component of foreshock dynamics. The phase speed of the large amplitude nonlinear waves exceeds the local Alfvén speed by the factor of 1.4–1.5 and the speed is positively correlated with the amplitude. The impact of the nonlinear waves on the background plasma has been quantified by the change of the pseudopotential, which shows a transition from a double well to a single well form. The presence of a double-well potential could, in principle, support a supernonlinear wave [33].

*B.Hnat@warwick.ac.uk

[1] C. F. Kennel, J. P. Edmiston, and T. Hada, *Collisionless Shocks in the Heliosphere: A Tutorial Review*, edited by R. G. Stone and B. T. Tsurutani (American Geophysical Union, Washington, D. C., 1985).
[2] S. J. Schwartz and D. Burgess, Geophys. Res. Lett. **18**, 1944 (1991).
[3] S. D. Bale *et al.*, Space Sci. Rev. **118**, 161 (2005).
[4] J. Giacalone, S. J. Schwartz, and D. Burgess, Ann. Geophys. **12**, 591 (1994).
[5] T. Dudok de Wit, V. V. Krasnosel'skikh, M. Dunlop, and H. Lühr, J. Geophys. Res. **104**, 17079 (1999).
[6] E. A. Lucek, T. S. Horbury, A. Balogh, I. Dandouras, and H. Réme, Ann. Geophys. **22**, 2309 (2004).
[7] D. Zhu, M. A. Balikhin, M. Gedalin, H. Alleyne, S. A. Billings, Y. Hobara, V. Krasnosel'skikh, M. W. Dunlop, and M. Ruderman, J. Geophys. Res. **113**, A04221 (2008).
[8] R. Behlke, M. Andr, S. D. Bale, J. S. Pickett, C. A. Cattell, E. A. Lucek, and A. Balogh, Geophys. Res. Lett. **31**, L16805 (2004).
[9] V. E. Zakharov, Zh. Eksp. Teor. Fiz. **62**, 1745 (1972) [Sov. Phys. JETP **35**, 908 (1972)].
[10] A. Hasegawa, Phys. Rev. A **1**, 1746 (1970).
[11] S. D. Bale, P. J. Kellogg, D. E. Larsen, R. P. Lin, K. Goetz, and R. P. Lepping, Geophys. Res. Lett. **25**, 1944 (1998).
[12] D. B. Graham, Y. V. Khotyaintsev, A. Vaivads, and M. André, Geophys. Res. Lett. **42**, 215 (2015).
[13] P. A. Robinson, Rev. Mod. Phys. **69**, 507 (1997).
[14] P. Kajdič, X. Blanco-Cano, E. Aguilar-Rodriguez, C. T. Russell, L. K. Jian, and J. G. Luhmann, J. Geophys. Res. **117**, A06103 (2012).
[15] J. R. Jokipii, Astrophys. J. **313**, 842 (1987).
[16] A. R. Bell, Mon. Not. R. Astron. Soc. **182**, 147 (1978).
[17] J. He, E. Marsch, C. Tu, S. Yao, and H. Tian, Astrophys. J. **731**, 85 (2011).
[18] T. Kukutani and H. Ono, J. Phys. Soc. Jpn. **26**, 1305 (1969).
[19] A. Rogister, Phys. Fluids **14**, 2733 (1971).
[20] V. B. Baranov and M. S. Ruderman, Fluid Dyn. **9**, 421 (1974).
[21] E. Mjolhus, Phys. Scr. **40**, 227 (1989).
[22] T. Hada, C. F. Kennel, and B. Buti, J. Geophys. Res. **94**, 65 (1989).
[23] E. Dubinin, K. Sauer, and J. F. McKenzie, J. Plasma Phys. **69**, 305 (2003).
[24] K. Sauer, E. Dubinin, and J. F. McKenzie, Geophys. Res. Lett. **29**, 3589 (2002).
[25] A. Balogh *et al.*, Space Sci. Rev. **79**, 65 (1997).
[26] H. Réme, Ann. Geophys. **19**, 1303 (2001).
[27] B. U. Sonnerup and M. Scheible, Analysis Methods for Multi-Spacecraft Data, edited by Gotz Paschmann and Patrick W. Daly, ISSI Scientific Report SR-001 (1998) (Electronic edition 1.1).
[28] N. E. Huang, Z. Shen, S. R. Long, M. C. Wu, H. H. Shih, Q. Zheng, N.-C. Yen, C. C. Tung, and H. H. Liu, Proc. R. Soc. A **454**, 903 (1998).
[29] Z. Wu and N. E. Huang, Adv. Adapt. Data Anal. **01**, 1 (2009).
[30] Y. Narita, K.-H. Glassmeier, S. Schafer, U. Motschmann, K. Sauer, I. Dandouras, K.-H. Fornacon, E. Georgescu, and H. Réme, Geophys. Res. Lett. **30**, 1710 (2003).
[31] V. M. Nakariakov *et al.*, Space Sci. Rev. **200**, 75 (2016).
[32] A. E. Dubinov and M. A. Sazonkin, J. Exp. Theor. Phys. **111**, 865876 (2011).
[33] A. E. Dubinov, D. Y. Kolotkov, and M. A. Sazonkin, Plasma Phys. Rep. **38**, 833844 (2012).